

Dynamics Reflect Gapless Edge Modes for Topological Superconductor

X.L. Zhao,^{1,2} M. Li,³ T.H. Qiu,³ L.B. Chen,² Y.L. Ma,³ H.Y. Ma*,³ and X.X. Yi*⁴

¹Graduate School of China Academy of Engineering Physics, China

²Quantum Physics Laboratory, School of Science,

Qingdao Technological University, Qingdao, 266033, China

³Qingdao University of Technology, 0532, Qingdao, Shandong, China

⁴Center for Quantum Sciences and School of Physics,
Northeast Normal University, Changchun 130024, China

(Dated: May 19, 2022)

We focus on the dynamical feature for a p -wave superconductor model in different parameter regions in terms of the appearance of gapless edge modes in reel geometry. Firstly, we show the parameter region with gapless edge modes versus a parameter and quasi-momentum. The parameter diagram can be reflected by the expectations of Pauli matrices in global manners. In another view, the dynamical feature of the excitation behave differently in the parameter regions with topological gapless edge modes and not. And the cusps of dynamical return rate vanish as the parameter pass the boundary in the parameter region slowly enough. It is found that the dynamics in the parameter region with gapless edge modes behaves differently to that without edge modes and related mostly to the eigenenergy gap between the pre-and post-quench eigenstates. The cusps of the dynamical return rate behave robustly against the noise in the lattice until localization behavior dominates. This work benefits detecting topological edge modes by dynamical manners.

I. INTRODUCTION

Different matter in one phase belong to the same equivalence class according to certain criteria. Distinct from Landau's theory about describing phase of matter based on order parameter, topological invariants act as new criteria in distinguishing phases of matter, like insulators, semimetals, and superconductors by a novel mechanism [1–3]. The topological p -wave superconductors which support gapless edge modes, are crucial for their implementation as ingredients for quantum-computing devices [4–8], and have attracted wide attention [9–11]. Such superconductors can be realized by depositing magnetic atoms on a conventional s -wave superconductor substrate [12, 13]. The topological phase can be characterized by topological invariants [14, 15]. We would focus on a topological superconductor model in this work.

Nonequilibrium phase transition is another novel topic attracting intensive attention which is also not based on the mechanism of Landau's order parameter theory about phase of matter. Such a phase transition occurs when quenching across the critical time for a transverse field Ising model [16] and quantum many-body spin system [19, 20]. These works inspire us to check the dynamical feature versus the appearance of topological gapless edge modes.

The homotopy invariant of loop constructed from time-evolution operator can represent the dynamical topology and opens up a novel avenue to classify quench dynamics [21]. Dynamically topological order is found closely related to the singularity of the Bogoliubov angle, but further investigation is needed for the quenches in the view of topology [22]. Topology-changing quenches have been investigated followed by dynamical phase transitions for various topological models [23]. The dynamical feature of localization-delocalization transition for a

one-dimensional incommensurate lattice described by the Aubry-André model has been investigated by quenching [24]. This inspires us checking the localization behavior during dynamics in this work.

In this work, we consider a topological superconductor model of reel geometry originated from Kitaev's model [5]. Firstly, the parameter region for the appearance of gapless edge modes is shown. The appearance of edge modes is also reflected by the expectations of Pauli matrices in global manners. Secondly, the dynamical properties in terms of gapless edge modes are checked including dynamical return rate, dynamics of excitations, and localization during evolution.

Following in Sec. II, the p -wave superconductor model which we focus on is introduced. In Sec. III, the parameter diagram in terms of the appearance of gapless edge modes and the relation with expectation values of Pauli matrices are studied. In Sec. IV, the dynamical feature for this model is checked. Finally, we conclude in Sec. V.

II. THE TOPOLOGICAL SUPERCONDUCTOR MODEL

We consider a two-dimensional topological p -wave superconductor model at the mean-field level described by the lattice Hamiltonian

$$\begin{aligned}
 H = & \sum_{n_x, n_y} -\mu a_{n_x, n_y}^\dagger a_{n_x, n_y} \\
 & - \kappa (a_{n_x, n_y}^\dagger a_{n_x+1, n_y} + a_{n_x, n_y}^\dagger a_{n_x, n_y+1} + h.c.) \quad (1) \\
 & + (\lambda_x a_{n_x, n_y}^\dagger a_{n_x+1, n_y}^\dagger + \lambda_y a_{n_x, n_y}^\dagger a_{n_x, n_y+1}^\dagger + h.c.),
 \end{aligned}$$

where n_x and n_y denote the positions for the sites in x and y directions on the lattice, respectively. The oper-

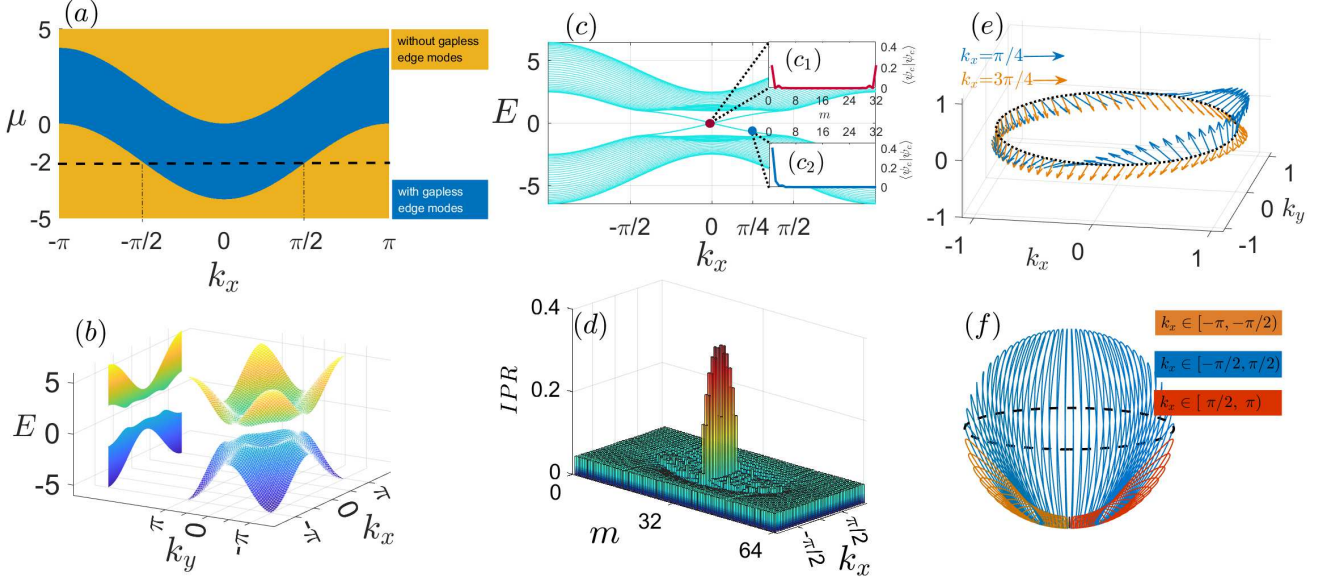


Figure 1. (a) The parameter diagram drawn according to Eq.(5), indicates the regions for the appearance of gapless edge modes for the reel-shape topological superconductor with periodic and open boundary conditions in x and y directions, respectively. The blue region denotes that with gapless edge modes and the other regions denote those without gapless edge modes. (b) Dispersion versus k_x and k_y with periodic boundary conditions in both x and y directions. (c) Branches of the dispersion relation versus k_x when $\mu = -2$, which is the main research situation in this work. The insets (c_1) and (c_2) show the distributions $\langle \psi_e | \psi_e \rangle$ for the edge modes $|\psi_e\rangle$ (half of the eigenstate is shown due to redundancy of the Hilbert space). (d) IPR for the eigenstates (numbered by m) versus k_x when $\mu = -2$. (e) The vector of $(\langle \sigma_x \rangle, \langle \sigma_y \rangle, \langle \sigma_z \rangle)$ for two examples in different parameter regions ($k_x = \pi/4$ and $k_x = 3\pi/4$) when $\mu = -2$ for a full period of k_y . (f) A range of trajectories for $(\langle \sigma_x \rangle, \langle \sigma_y \rangle, \langle \sigma_z \rangle)$ when the trajectories are drawn of $k_y \in [-\pi, \pi)$ for three regions of $k_x \in [-\pi, -\pi/2)$, $[-\pi/2, \pi/2)$, $[\pi/2, \pi)$ with different dominant colors (slightly gradient color for different k_x).

ator a_{n_x, n_y} (a_{n_x, n_y}^\dagger) annihilates (creates) a fermion on the lattice site with the coordinate (n_x, n_y) . μ is the chemical potential. Such a quantity in one dimensional topological superconductor corresponds to external magnetic field when it is transformed to the transverse-field XY model by Jordan-Wigner transformation [25, 26]. κ is the hopping matrix element used as the unit in this work ($\kappa=1$) and $\lambda_{x(y)} = \lambda_0 e^{i\theta_{x(y)}}$. We focus on the case $\lambda_0=1/2$, $\theta_{x(y)}=0(\pi/2)$ in this work. Namely, the pairing amplitude is anisotropic with an additional phase of $\pi/2$ in y -direction compared to x -direction. It is a spin-polarized fermion model with the spin degree of freedom frozen by magnetic field.

After the Fourier transformation in x and y directions, we obtain the Hamiltonian in the quasi-momentum space

$$\begin{aligned} \mathcal{H} &= \sum_{\alpha=x,y,z} h_\alpha \sigma_\alpha \\ &= \sum_{k_x, k_y} (\sin k_y - i \sin k_x) \sigma_+ + h.c. + \xi_k \sigma_z, \end{aligned} \quad (2)$$

where $\sigma_\pm = (\sigma_x \pm i\sigma_y)/2$. $\sigma_{x,y,z}$ are Pauli matrices and $\xi_k = -2(\cos k_x + \cos k_y) - \mu$ with 4κ shifted without loss of generality. Note that \mathcal{H} has particle-hole symmetry but no time-reversal symmetry. It is a two-dimensional representation of symmetry class- D describing Z topo-

logical superconductor according to the 10-fold classification [27, 28]. Due to geometrical symmetry, we consider the periodic and open boundary conditions in x and y directions, respectively. This is a reel model closing a strip lattice to a cylinder surface with only Fourier transformation taken in x direction. Then the Hilbert space is redundantly expanded by the particle-hole basis $\phi_{k_x}^\dagger = (a_{k_x,1}^\dagger, a_{-k_x,1}, a_{k_x,2}^\dagger, a_{-k_x,2}, \dots, a_{k_x, N_y}^\dagger, a_{-k_x, N_y})$, where $a_{k_x, n_y} = \frac{1}{\sqrt{2N_x}} \sum_{n_x=1}^{N_x} a_{n_x, n_y} e^{ik_x n_x}$. We would focus on the parameter diagram about the appearance of gapless edge modes, and the corresponding dynamical feature for this model.

III. THE PARAMETER DIAGRAM

In this work, we take periodic boundary condition along x direction and open boundary condition along y direction. Then k_x acts as a good quantum number. The topological phase can be reflected by integrals [29–31]. For example, the integral in the Brillouin zone (FBZ): $\sigma_{xy} = \frac{1}{4\pi} \iint_{FBZ} \hat{h} \cdot (\partial_{k_x} \hat{h} \times \partial_{k_y} \hat{h}) dk_x dk_y$, where \hat{h} is the normalized vector of (h_x, h_y, h_z) in the Eq.(2) [30]. After some algebra, one can find $\sigma_{xy} = \frac{1}{4\pi} \iint_{FBZ} \hat{n} \cdot (\partial_{k_x} \hat{n} \times \partial_{k_y} \hat{n}) dk_x dk_y$, where \hat{n} is the normalization for

$(\langle\sigma_x\rangle, \langle\sigma_y\rangle, \langle\sigma_z\rangle)$ under the ground state [29, 31]. These calculations can be examined by using the ground state in the eigen-equations for the Hamiltonian (2) as below

$$\mathcal{H}|\pm\rangle = \pm\Omega|\pm\rangle, \quad (3)$$

where $\Omega = \sqrt{h_x^2 + h_y^2 + h_z^2}$, and

$$|\pm\rangle = \frac{\pm 1}{\sqrt{2\Omega(\Omega \pm h_z)}} \begin{bmatrix} h_x - ih_y \\ -h_z \mp \Omega \end{bmatrix}. \quad (4)$$

After calculating σ_{xy} , it can be verified that the topological nontrivial parameter interval is $\mu \in (-4, 4)$.

In topological classification of matter, bulk-boundary correspondence is a remarkable characteristic. The appearance of topological gapless edge modes is a signature for topological phase. As we focus on reel-shape lattice, we pay special attention on the parameter region with the appearance of the gapless edge modes versus μ and k_x as shown in FIG. 1(a). We found that the gapless edge modes locate between the parameter boundaries described by the relations:

$$\mu = -2 \cos k_x \pm 2. \quad (5)$$

The region for the appearance of the topological gapless edge modes is coincident with FIG. 1(a) shown by a cartoon in the supplementary material [32].

To check the details of the topological edge modes, the eigenenergy spectra in quasi-momentum space (with Fourier transformation taken only in x and y directions) and a reel-shape geometry (with Fourier transformation taken only in x direction) are shown in FIG. 1 (b) and (c), respectively. The subfigures FIG. 1 (c_1) and FIG. 1(c_2) show the halves for the two distributions of the edge modes.

The topological edge modes have remarkable localization characteristic compared to ordinary modes. The localization for an state can be revealed by the quantity $IPR = \sum_j^{N_y} |\psi_j^{m, k_x}|^4$, here ψ_j^{m, k_x} denotes the projection of the m th eigenstate on the j th site for certain k_x [33]. The localization for the eigenstates identified by m versus k_x are shown in FIG. 1(d). It can be seen that the region for the appearance of the gapless edge modes is consistent with the parameter diagram in FIG. (1)(a) and (c).

Topological phase of matter is usually indicated by the invariants like Zak phase, Chern number and so on. In this work, the expectations of Pauli matrices under ground state, namely, $\langle\sigma_x\rangle$, $\langle\sigma_y\rangle$, and $\langle\sigma_z\rangle$ can also be applied to distinguish different parameter regions in terms of gapless edge modes. For example, the vector of $(\langle\sigma_x\rangle, \langle\sigma_y\rangle, \langle\sigma_z\rangle)$ plays such a role for this model shown in FIG. 1(e). A reference loop is parameterized as $(\cos k_x, \sin k_y)$. The vectors wind this loop a full round when there is topological gapless edge modes ($k_x = \pi/4$ as an example) whereas not when there is no gapless edge modes ($k_x = 3\pi/4$ as an example), obtained for k_y being ergodic $(-\pi, \pi]$. This agrees with FIG. 1(a) and (c). Besides, the trajectories of $\langle\sigma_x\rangle - \langle\sigma_y\rangle - \langle\sigma_z\rangle$ form different

loops in terms of the appearance of gapless edge modes on the Bloch sphere as shown in FIG. 1(f). These results suggest that the appearance of topological gapless edge modes can be revealed by expectation values of operators in global manners. This benefits checking the topological phase of matter in experiments.

IV. DYNAMICAL FEATURE

Since the appearance of gapless edge modes is a remarkable signature for topological phase of matter and the structure of energy band is related to the dynamics of the excitations in lattices. One may conjecture that the presence of gapless edge modes may be reflected by the dynamics of excitations. Thus, we check the dynamical features versus the appearance of gapless edge modes, including quenching by turning the parameter μ suddenly and the evolution of the excitation in different parameter regions in the following.

A. Quenching

In conventional thermodynamics and statistical physics, non-analyticities of free energy density at critical temperatures indicate phase transition in thermodynamic limit. Similarly, dynamical phase transition describes the analog behavior occurs in quantum systems when time evolution acts as temperature variation with non-analytic behavior during evolution. Quenching is a candidate to reflect the dynamical phase transition by instantaneously changing the parameter(s) of a Hamiltonian starting from a ground state [16, 22, 23]. The Loschmidt overlap defined as

$$G(t) = |\langle\psi_{\mu;0}|e^{-iH't}|\psi_{\mu;0}\rangle|, \quad (6)$$

is a quantity applied in quench. $|\psi_{\mu;0}\rangle$ denotes the initial state with parameter μ in the Hamiltonian. This quantity measures the overlap between the time evolved state $e^{-iH't}|\psi_{\mu;0}\rangle$ and the initial state $|\psi_{\mu;0}\rangle$ following a sudden change of the parameter μ in the post-quench Hamiltonian, namely, $H(\mu) \xrightarrow{\text{quench}} H(\mu')$ in this work.

In statistical physics, the zeros of a partition function correspond to the cusps of free energy density in thermodynamic limit as a function of temperature. Similarly, the Loschmidt overlap in Eq.(6) plays the role as the partition function [16]. Since $G(t)$ scales with the size of the system N , another quantity, return rate is usually employed in quenching

$$f(t) = -\frac{1}{N} \ln G(t). \quad (7)$$

[16, 34]. This quantity behaves non-analytically versus time when the Loschmidt overlap $G(t)$ vanishes. We employ this quantity to check the dynamics in terms of the

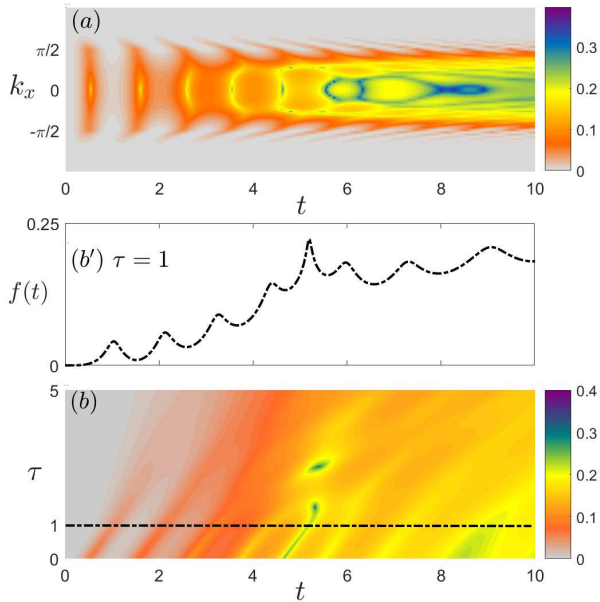


Figure 2. (a) $f(t)$ as a function of time t and k_x when $\mu = -2$. (b) $f(t)$ versus time t and τ introduced in Eq.(8) when $k_x = \pi/4$. (b') shows $f(t)$ versus time when $\tau = 1$ corresponding to the dash-dotted line in (b).

appearance of gapless edge modes. $f(t)$ is shown versus time t and k_x in FIG. 2(a) when μ changes suddenly from -2 to -5 . While $\mu = -2$ and $k_x \in (-\pi/2, \pi/2)$ in the Brillouin zone, the gapless edge modes appear, and when k_x belongs to the complementary set, the gapless edge modes disappear, as shown in FIG. 1 (c). While $\mu = -5$, this model is in the topologically trivial phase in the whole Brillouin zone without gapless edge modes. As can be seen in FIG. 2(a), the behavior of $f(t)$ is different obviously whether or not μ quenching across the parameter boundary of the regions with and without gapless edge modes.

Besides the sudden change of parameters in quench, it is natural to consider what happens if the parameter μ continuously crossing such parameter boundaries within finite time. Among various manners of the parameter crossing the boundaries, we consider the case

$$\mu(t) = \begin{cases} \mu_0 + \frac{(\mu_f - \mu_0)t}{\tau} & t \leq \tau, \\ \mu_f & t > \tau, \end{cases} \quad (8)$$

$\mu_f = -5$ and $\mu_0 = -2$ in this work. The larger τ is, the further it from quenching and the closer to adiabatic process. The results are shown in FIG. 2 (b). It can be seen that the cusps appear and delay until τ becomes too large. The slower $\mu(t)$ crossing the parameter boundaries, the latter the cusps appear since it takes time for reaching the boundary. Different response for the quench across the parameter boundary may provide the reference to design control strategies to finish certain research for this model.

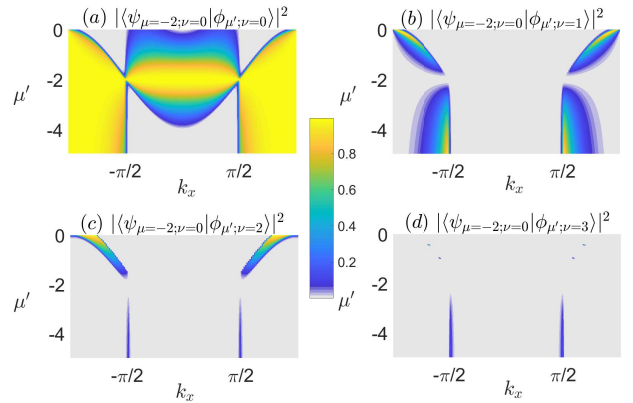


Figure 3. (a)-(d) $|\langle \psi_{\mu=-2; \nu=0} | \phi_{\mu'; \nu} \rangle|^2$ as a function of k_x and μ' for $\nu=0,1,2,3$, respectively. $|\psi_{\mu=-2; \nu=0}\rangle$ is the ground state of the pre-quench Hamiltonian and $|\phi_{\mu'; \nu}\rangle$ are the eigenstates of the post-quench Hamiltonian when the chemical potential is μ' . The eigenstates with larger ν denote those with eigenvalues further from the one corresponding to $|\psi_{\mu=-2; \nu=0}\rangle$.

B. Overlap between Eigenstates

We conjecture the overlap between the eigenstates of the post-quench Hamiltonian and the initial state (pre-quench) ($|\psi_{\mu=-2; \nu=0}\rangle$) is a critical factor influencing the appearance of the cusps during the evolution. Here ν is the number for different eigenstates. Thus we check the projection $|\langle \psi_{\mu=-2; \nu=0} | \phi_{\mu'; \nu} \rangle|^2$, where $|\phi_{\mu'; \nu}\rangle$ are the eigenstates of the post-quench Hamiltonian with the parameter μ having changed to μ' abruptly. This projection measures the distance between $|\psi_{\mu=-2; \nu=0}\rangle$ and $|\phi_{\mu'; \nu}\rangle$. The larger ν corresponds to the larger eigenenergy gap between the corresponding eigenenergies of $|\psi_{\mu=-2; \nu=0}\rangle$ and $|\phi_{\mu'; \nu}\rangle$. The results are shown in FIG. 3. Comparing FIG. 3 (a) with FIG. 1 (a), the projection $|\langle \psi_{\mu=-2; \nu=0} | \phi_{\mu'; \nu=0} \rangle|^2$ approaches zero when μ changes from the region with (without) gapless edge modes to that without (with) such modes. By comparing FIG.3 (a)-(d), when it quenches to the same parameter region, the distribution of $|\langle \psi_{\mu=-2; \nu=0} | \phi_{\mu'; \nu} \rangle|^2$ take largest values when $\nu = 0$. Since larger ν denotes the eigenstate with an eigenvalue further from the one corresponding to $|\psi_{\mu=-2; \nu=0}\rangle$. Those distributions of $|\langle \psi_{\mu=-2; \nu=0} | \phi_{\mu'; \nu} \rangle|^2$ with larger ν show weaker correlation to whether it quenches to different parameter regions. Thus, it means the eigenstate with the nearest eigenenergy in the post-quench Hamiltonian is correlated prominently to the cusps in the dynamics.

C. Dynamical Features in Different Parameter Regions

The dynamical feature of excitations may behave distinctively in different parameter regions in terms of the appearance of gapless edge modes. To examine this, we

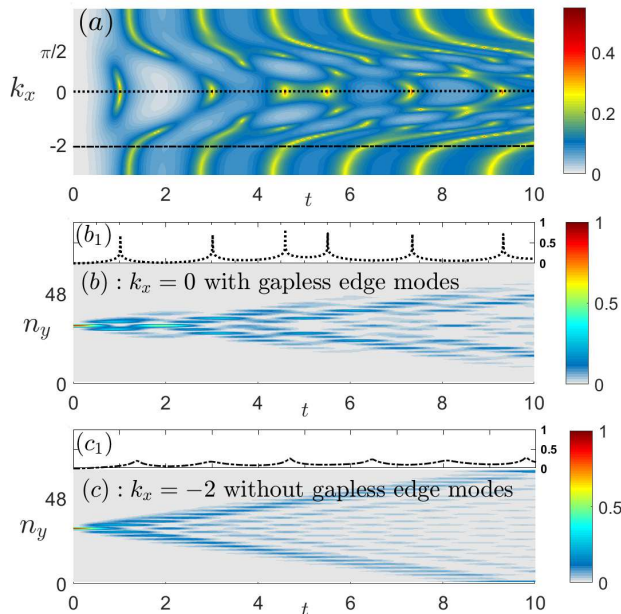


Figure 4. (a) $f'(t)$ versus time t and k_x starting from the initial state with all population on the middle of the lattice. The other parameters in the Hamiltonian are same to those in FIG. 2. (b) and (c) show the projections of the excitation on the lattice during evolution when $k_x=0$ (with gapless edge modes) and -2 (without gapless edge modes), respectively. And a full examination of k_x in the Brillouin zone is in the supplementary material [35]. (b₁) and (c₁) show the corresponding $f'(t)$ for (b) and (c), respectively.

employ a quantity $f'(t)$ with the definition formally like the return rate $f(t)$, and the projection of the excitation on the lattice site during evolution in different parameter regions in FIG. 4. It should be emphasized that, here we do not use an eigenstate of the pre-quench Hamiltonian as the initial state in $f'(t)$, but the excitation with full population on one site as the initial state. As shown in FIG. 4 (b) and (c), the free dynamics of the excitation behaves distinctively in different parameter regions in terms of edge modes. And a full range of examination is in the supplementary material [35]. The results hint that the dynamics of the excitation provides a candidate to denote parameter regions with gapless edge modes or not.

D. Localization Resulting from Noise

Noise and disorders are usually inevitable in reality. The robust property against disorders of topological edge modes makes them be potential ingredients for quantum computation. As mentioned previously, the appearance of the gapless edge modes is related to the appearance of cusps in $f(t)$. We explore the behavior of $f(t)$ in the presence of the time-dependent noise in μ after quenching from the region with gapless edge modes to that

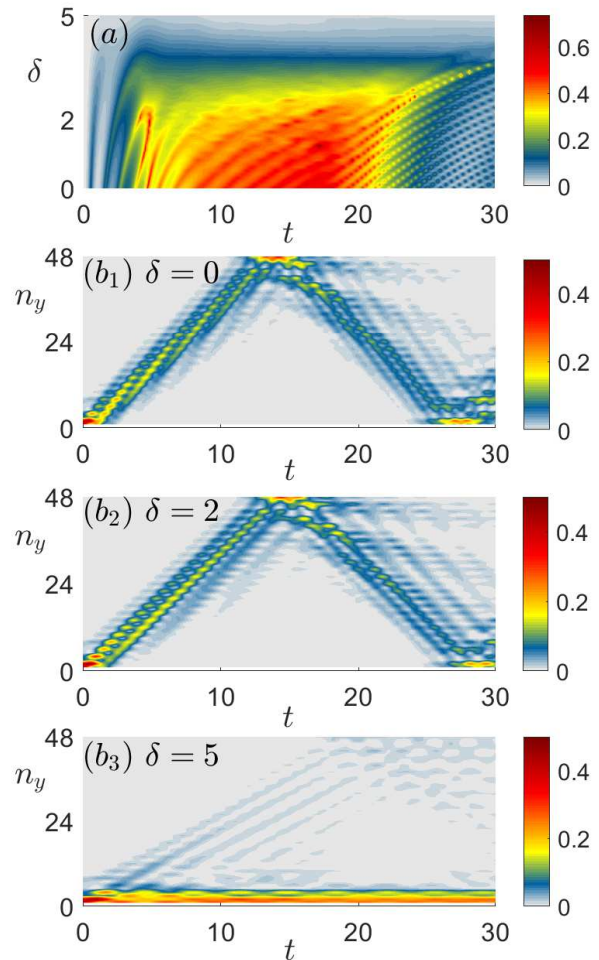


Figure 5. (a) $f(t)$ versus the amplitude δ of the noise and time t when $N_y=24$ and $k_x=\pi/4$. The other parameters are same to those in FIG. 2. (b₁)-(b₃) show the dynamics of the excitations when the noise amplitude $\delta=0, 2$ and 5 , respectively.

without gapless edge modes. The noise is introduced as $\mu_\delta(t)=\mu+\delta\mu(t)$, where $\delta\mu(t)$ denotes the fluctuation with values randomly distributed in $[0, \delta]$ during evolution. Different from the noise in thermodynamics and statistical physics which denotes the thermal vibration of the particles and leads to thermalization, this noise results from the random vibration of the lattice. In FIG. 5 (a), we show the dynamics of $f(t)$ versus δ and time. It can be seen that cusps occurs until the noise makes $\mu_\delta(t)$ cross the parameter boundary between regions with and without gapless edge modes as shown in FIG. 5 (a).

To check the influence of the noise on the dynamics in detail, three examples of the dynamics quenching from the gapless edge modes are shown in FIG. 5 (b₁) – (b₃). The dynamics is depressed, and localization occurs as the excitation is mainly bounded near the edge with δ increasing. Meanwhile, the cusps in $f(t)$ vanish meanwhile the dynamical pattern changes to those in the re-

gion without gapless edge modes, like that in FIG. 4 (c).

Disorders in real space lead to localization of quantum states due to Anderson localization mechanism [36]. This provides the clue to get insight into the mechanism of the above localization in future works. However, if the noise becomes too large, it is beyond the scope of this mean-field model in this work. The above result also hints that the topological phase can be reflected by dynamics.

V. CONCLUSION

The parameter diagram and the dynamical features in terms of the appearance of topological gapless edge modes have been explored for a topological superconductor model with periodic and open boundary conditions in two orthogonal directions. The appearance of the gapless edge modes can be reflected by the expectations of Pauli matrices in two global manners. The dynamical feature of excitations behave distinctively in terms of the appear-

ance of gapless edge modes and related mostly to the states with proximate eigenenergy between the pre- and post-quench Hamiltonians. The cusps in the return rate occurs until the parameter passes the parameter boundary very slowly. The dynamical pattern of the excitation in the region with gapless edge modes is different to that in the region without gapless edge modes. The cusps behave robustly until the noise of the lattice leads to topological phase transition. This work indicates one can detect topological phase in dynamical manners.

VI. ACKNOWLEDGEMENTS

X.L. Zhao thanks National Natural Science Foundation of China, No.12005110, 11975132, Natural Science Foundation of Shandong Province, China, No.ZR2020QA078, ZR2021LLZ001, and Project of Shandong Province Higher Educational Science and Technology Program, No.J18KZ012.

-
- [1] J.M. Kosterlitz and D.J. Thouless, J. Phys. C: Solid State Phys. **6**, 1181 (1973).
 - [2] D.J. Thouless, M. Kohmoto, M.P. Nightingale, and M. den Nijs, Phys. Rev. Lett. **49**, 405 (1982).
 - [3] F.D. M. Haldane, Phys. Rev. Lett. **50**, 1153 (1983).
 - [4] N. Read and D. Green, Phys. Rev. B **61**, 10267 (2000).
 - [5] A.Y. Kitaev, Phys.-Usp **44**, 131 (2000).
 - [6] D.A. Ivanov, Phys. Rev. Lett. **86**, 268 (2001).
 - [7] J. Alicea, Rep. Prog. Phys. **75**, 076501 (2012).
 - [8] B. Andrei Bernevig and T.L. Hughes, *Topological Insulators and Topological Superconductors* (Princeton University Press, Princeton, 2013).
 - [9] M. Sato, Y. Takahashi, S. Fujimoto, Phys. Rev. Lett. **103**, 020401 (2009).
 - [10] J.D. Sau, R.M. Lutchyn, S. Tewari, and S.D. Sarma, Phys. Rev. Lett. **104**, 040502 (2010).
 - [11] J. Alicea, Phys. Rev. B **81**, 125318 (2010).
 - [12] S. Nadj-Perge, I.K. Drozdov, J.Li, H. Chen, S. Jeon, J. Seo, A.H. MacDonald, B.A. Bernevig, and A. Yazdani, Science **346**, 602 (2014).
 - [13] R. Pawlak, M. Kisiel, J. Klinovaja, T. Meier, S. Kawai, T. Glatzel, D. Loss, and E. Meyer, npj Quantum Inf **2**, 16035 (2016).
 - [14] T.H. Hansson, V. Oganesyan, S.L. Sondhi, Annals of Physics, **313**, 497 (2004).
 - [15] C.L. Kane and E.J. Mele, Phys. Rev. Lett. **95**, 146802 (2005).
 - [16] M. Heyl, A. Polkovnikov, and S. Kehrein, Phys. Rev. Lett. **110**, 135704 (2013).
 - [17] M.E. Fisher, *Lectures in Theoretical Physics. Vol. 7C: Statistical Physics, Weak Interactions, Field Theory: Lectures Delivered at the Summer Institute for Theoretical Physics, University of Colorado, Boulder, 1964* (University of Colorado Press, 1965).
 - [18] I. Bena, M. Droz, and A. Lipowski, Int. J. Mod. Phys. B **19**, 4269 (2005).
 - [19] P. Jurcevic, H. Shen, P. Hauke, C. Maier, T. Brydges, C. Hempel, B.P. Lanyon, M. Heyl, R. Blatt, and C.F. Roos, Phys. Rev. Lett. **119**, 080501 (2017).
 - [20] T. Tian, H.-X. Yang, L.-Y. Qiu, H.-Y. Liang, Y.-B. Yang, Y. Xu, and L.-M. Duan, Phys. Rev. Lett. **124**, 043001 (2020).
 - [21] H. Hu, E. Zhao, Phys. Rev. Lett. **124**, 160402 (2020).
 - [22] C. Ding, Phys. Rev. B **102**, 060409(R) (2020).
 - [23] S. Vajna and B. Dóra, Phys. Rev. B **91**, 155127 (2015).
 - [24] C. Yang, Y.C. Wang, P. Wang, X.L. Gao, and S. Chen, Phys. Rev. B **95**, 184201 (2017).
 - [25] E. Barouch, B.M. McCoy, and M. Dresden, Phys. Rev. A **2**, 1075 (1970).
 - [26] L.C. Venuti, N.T. Jacobson, S. Santra, and P. Zanardi, Phys. Rev. Lett. **107**, 010403 (2011).
 - [27] A. Altland and M.R. Zirnbauer, Phys. Rev. B **55**, 1142 (1997).
 - [28] A.P. Schnyder, S. Ryu, A. Furusaki, and A.W.W. Ludwig, Phys. Rev. B **78**, 195125 (2008).
 - [29] F. Wilczek and A. Zee, Phys. Rev. Lett. **51**, 2250 (1983).
 - [30] X.L. Qi, Y.S. Wu, and S.C. Zhang, Phys. Rev. B **74**, 085308 (2006)
 - [31] J. E. Moore, Y. Ran, and X.G. Wen, Phys. Rev. Lett. **101**, 186805 (2008).
 - [32] The file “Eq3.avi” shows the region for the appearance of topological gapless edge modes described by Eq. 5.
 - [33] D.J. Thouless, Phys. Rep. **13**, 93 (1974).
 - [34] B. Pozsgay, J. Stat. Mech. P10028 (2013).
 - [35] The file “Evolution.avi” shows the full examination of the projection on the lattice in parameter regions with and without gapless edge modes.
 - [36] P.W. Anderson, Phys. Rev. **109**, 1492 (1958).